Structure of Polydisperse Inverse Ferrofluids: Theory and Computer Simulation

Y. C. Jian, Y. Gao, and J. P. Huang*

Surface Physics Laboratory and Department of Physics, Fudan University, Shanghai 200433, China

R. Tao

Department of Physics, Temple University, Philadelphia, Pennsylvania 19122

Received: July 25, 2007; In Final Form: October 18, 2007

By using theoretical analysis and molecular dynamics simulations, we investigate the structure of colloidal crystals formed by nonmagnetic microparticles (or magnetic holes) suspended in ferrofluids (called inverse ferrofluids), by taking into account the effect of polydispersity in size of the nonmagnetic microparticles. Such polydispersity often exists in real situations. We obtain an analytical expression for the interaction energy of monodisperse, bidisperse, and polydisperse inverse ferrofluids. Body-centered tetragonal (bct) lattices are shown to possess the lowest energy when compared with other sorts of lattices and thus serve as the ground state of the systems. Also, the effect of microparticle size distributions (namely, polydispersity in size) plays an important role in the formation of various kinds of structural configurations. Thus, it seems possible to fabricate colloidal crystals by choosing appropriate polydispersity in size.

I. Introduction

In recent years, inverse ferrofluids with nonmagnetic colloidal microparticles suspended in a host ferrofluid (also called magnetic fluid)[1−3] have drawn considerable attention for its potential application in its industrial applications and potential use in biomedicine.[4−11] The sizes of the nonmagnetic microparticles are about 1∼100 μm (which can easily be made in experiments) such as polystyrene microparticles. The inverse ferrofluid system can be modeled in a dipolar interaction approximation. Here, the dipolar interaction approximation is actually the first-order approximation of multipolar interaction. Because the nonmagnetic microparticles are much larger than the ferromagnetic nanoparticles in a host ferrofluid, the host can theoretically be treated as a uniform continuum background in which the much larger nonmagnetic microparticles are embedded. If an external magnetic field is applied to the inverse ferrofluid, the nonmagnetic microparticles suspended in the host ferrofluid can be seen to possess an effective magnetic moment but opposite in direction to the magnetization of the host ferrofluid. As the external magnetic field increases, the nonmagnetic microparticles aggregate and form chains parallel with the applied magnetic field. These chains finally aggregate to a column-like structure, completing a phase transition process, which is similar to the cases of electrorheological fluids and magnetorheological fluids under external electric or magnetic fields. The columns can behave as different structures like body-centered tetragonal (bct) lattices, face centered cubic (fcc) lattices, hexagonal close packed (hcp) lattices, and so on. In this work, we assume that the external magnetic field is large enough to form different lattice structures. The actual value of the external magnetic field needed to form such structures is related to the volume fraction of the nonmagnetic microparticles and the magnetic properties of the host ferrofluid.

In this work, we shall use the dipole-multipole interaction model[12] to investigate the structure of inverse ferrofluids. In ref 12, Zhang and Widom discussed how the geometry of elongated microparticles will affect the interaction between two droplets and introduced higher multipole moments' contribution by using a dipole and multipole (dipole−multipole) interaction model to give a more exact expression of interaction energy than using the dipole and dipole (dipole−dipole) interaction model. The leading dipole−dipole force does not reflect the geometry relation between the microparticles nearby, while the dipole−multipole model includes the contributions from the size mismatch and is simpler and more practical than the multipolar expansion theory[13,14] in dealing with the complex interaction between microparticles for its accuracy. Size distributions can be regarded as a crucial factor which causes depletion forces in colloidal droplets.[15] Even though researchers have tried their efforts to fabricate monodisperse systems for obtaining optimal physical or chemical properties,[16,17] polydispersity in size of microparticles often exists in real situations,[18−22] since the microparticles always possess a Gaussian or log-normal distribution. Here, we consider size distributions as an extra factor affecting the interaction energy. Polydisperse ferrofluid models are usually treated in a global perspective using chemical potential or free energy methods,[6,23,24] while the current model concerns the local nature in the crystal background. A brief modeling is carried out for the size distribution picture in the formation of crystal lattices. The purpose of this paper is to use this model to treat the structure formation in monodisperse, bidisperse, and polydisperse inverse ferrofluids, thus yielding theoretical predictions for the ground state for the systems with or without microparticle size distributions (or polydispersity in size). It is found that when the size mismatch is considered between the microparticles, the interaction between them becomes complex and sensitive to the different configurations. This method can also be extended to other ordered configurations in polydisperse crystal systems.

This paper is organized as follows. In section II, based on the dipole−multipole interaction model, we present the basic two-microparticle interaction model to derive interaction po-

* Corresponding author. E-mail: jphuang@fudan.edu.cn.

10.1021/jp075849h CCC: $40.75
Published on Web 12/21/2007

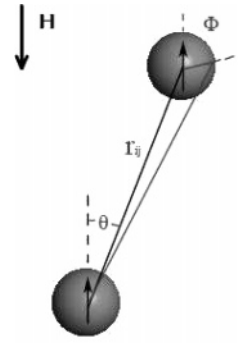

Figure 1. Schematic graph showing two nonmagnetic microparticles (magnetic hole) of radius r_1 and r_2, suspended in a ferrofluid under an applied magnetic field H.

tentials. In sections III and IV, we apply the model to three typical structures of colloid crystals formed in inverse ferrofluids and then investigate the ground state in two different configurations by taking into account the effect of size distributions. As an illustration, in section V, we perform molecular dynamics simulations to give a picture of the microparticle size distribution in the formation of a bct lattice in bidisperse inverse ferrofluids. The paper ends with a discussion and conclusion in section VI.

II. Interaction Model for Two Nonmagnetic Microparticles

We start by considering a simple situation in which two nonmagnetic spherical microparticles (also called magnetic holes) are put nearby inside a ferrofluid which is homogeneous at the scale of a sphere in an applied uniform magnetic field H, see Figure 1. The nonmagnetic microparticles create holes in the ferrofluid, and corresponding to the amount and susceptibility of the ferrofluid, they possess the effective magnetic moment, which can be described by[25] $\mathbf{m} = -\chi_f/(1 + 2/3\chi_f)V\mathbf{H} = -\chi V\mathbf{H}$, where χ_f (or χ) means the magnetic susceptibility of the host (or inverse) ferrofluid. When the two nonmagnetic microparticles placed together with distance r_{ij} away, we can view the magnetization in one sphere (labeled as A) as induced by the second (B). The central point of dipole−multipole technique is to treat B as the dipole moment m at the first place and then examine the surface charge density Σ induced on the sphere A. From Σ, we can use the multipole expansion (detailed discussion can be found in ref 26) to obtain the multipole moment. When exchanging the status of A and B, treating A as the dipole moment, the averaged force between the two microparticles is thus obtained. For the perturbation of the magnetic field due to the two microparticles, magnetization M in the microparticles becomes nonuniform, and they will obtain multipole moments from mutual induction. However, the bulk magnetic charge density still satisfies $\rho = \nabla\cdot\mathbf{M} = 0$. So we need only study the surface charge Σ_n,

$$\sum_n = \hat{\mathbf{n}}\cdot\mathbf{M} \tag{1}$$

where $\hat{\mathbf{n}}$ is the unit normal vector pointing outward. The magnetic multipole moments by surface charge density in spherical coordinates can be written as,

$$q_{ln} = \int Y^*_{ln}(\phi, \varphi) r_1^l \sum_n \mathrm{d}S \tag{2}$$

where r_1 denotes the radius of the microparticle. All $n \neq 0$ moments vanish because of rotational symmetry about the direction of magnetization; so, eq 2 can be rewritten as

$$A_l \equiv q_{l0} = \sqrt{(2l+1)\pi}\int_{-1}^{1} P_l(\cos\phi) r_1^{l+2} \sum_n (\cos\phi)\mathrm{d}\cos\phi \tag{3}$$

We can expand the surface charge density in Legendre polynomials in the spherical coordinates (r, ϕ, φ),[12]

$$\sum_n (\cos\phi) = \frac{\chi}{r_{ij}^3}\sum_{l=1}^{\infty}(-1)^{l+1} l(l+1)\left(\frac{r_1}{r_{ij}}\right)^{l-1} P_l(\cos\phi) \tag{4}$$

The $l \geq 2$ parts in eq 4 correspond to the effects of multipole (that are beyond the dipole). Here, we set spherical harmonics $\int_0^{2\pi}\mathrm{d}\varphi \int_0^{\pi}\sin\phi Y^*_{l',n'}(\phi, \varphi) Y_l(\phi, \varphi)\,\mathrm{d}\phi = \delta_{l',l}\delta_{n',n}$. The force between the dipole moment m and induced multipole moment A_l can be derived as

$$F_{D-M} = (-1)^l(l+1)(l+2)\left(\frac{4\pi}{2l+1}\right)^{1/2}\frac{mA_l}{r_{ij}^{l+3}}\cos\phi \tag{5}$$

In view of the orthogonal relation $\int_{-1}^{1} P_l^n P_{l'}^n\,\mathrm{d}x = [2/(2l+1)][(l+n)!/(l-n)!]\delta_{ll'}$, we obtain the interaction energy for the dipole-multipole moment

$$U_{D-M} = \frac{\pi}{4}\mu_f m_1 m_2 \sum_l \frac{\pi}{2}\chi\frac{l(l+1)^2}{2l+1}(r_1^{2l+1} + r_2^{2l+1})\frac{1-3\cos^2\theta}{r_{ij}^{2l+4}} = \mu\sum_l f(l)\frac{1-3\cos^2\theta}{r_{ij}^{2l+4}} \tag{6}$$

where $\mu = (\pi/4)\mu_f m_1 m_2$, $f(l) = (\pi/2)\chi[l(l+1)^2/2l+1](r_1^{2l+1} + r_2^{2l+1})$, the suffix D (M) of force F or energy U stands for the dipole moment (multipole moment), and magnetic permeability $\mu_f = \mu_0(1 + \chi_f)$ with $\mu_0 = 4\pi \times 10^{-7}$ $\mathbf{H}\cdot\mathbf{m}^{-1}$. Here, m_1 and m_2 denote the effective magnetic moments of the two nonmagnetic microparticles, which is induced by external field as dipolar perturbation. $0 \leq \theta \leq \pi/2$ is the angle between the their joint line with the direction of external field, and ϕ and φ are both the spherical coordinates (r, ϕ, φ) for one single nonmagnetic microparticle. For typical ferrofluids, there are magnetic susceptibilities, $\chi_f = 1.9$ and $\chi = 0.836$.[23] Because we consider the bct, fcc, and hcp lattices, the crystal rotational symmetry in the xy plane is fourfold, and the value of n can only be 0, ±4, ... In the general case, when the polarizabilities between the microparticles and the ambient fluid is low, the higher magnetic moments can be neglected since they contribute less than 5% of the total energy.[12] In this picture, the nonmagnetic microparticle pair reflects the dipole−dipole and dipole−multipole nature of the interaction and can be used to predict the behavior of microparticle chains in simple crystals.

III. Possible Ground State for Uniform Ordered Configurations

Let us first consider a bidisperse model which has been widely used in the study of magnetorheological fluids and ferrofluids. The model has a large amount of spherical nonmagnetic microparticles with two different sizes suspended in a ferrofluid which is confined between two infinite parallel nonmagnetic

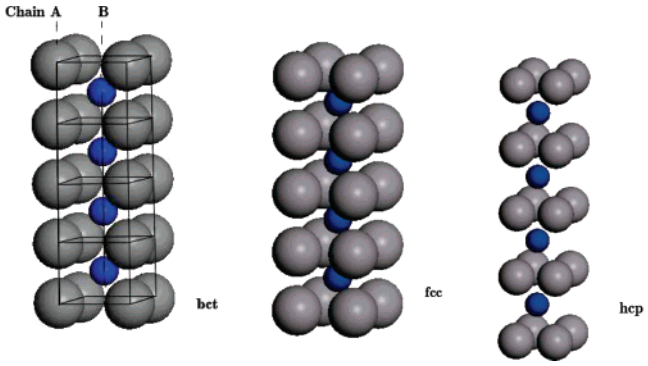

Figure 2. Three different lattices, bct, fcc, and hcp, which are composed of nontouching microparticles with different size distribution.

plates with positions at $z = 0$ and $z = L$, respectively. When a magnetic field is applied, dipole and multipole moments will be induced to appear in the spheres. The inverse ferrofluid systems consist of spherical nonmagnetic microparticles in a carrier ferrofluid, and the viscosity of the whole inverse ferrofluid increases dramatically in the presence of an applied magnetic field. If the magnetic field exceeds a critical value, the system turns into a solid whose yield stress increases as the exerting field is further strengthened. The induced solid structure is supposed to be the configuration minimizing the interaction energy, and here, we assume first that the microparticles with two different sizes have a fixed distribution as discussed below.

By using the cylindrical coordinates, the interaction energy between two microparticles labeled as i and j considering both the dipole−dipole and the dipole−multipole effects can be written as

$$U_{ij}(\rho, z) = \mu\left(1 + \sum_l \frac{f(l)}{r_{ij}^{2l+1}}\right)\cdot\left(\frac{1 - 3\cos^2\theta}{r_{ij}^{3}}\right) \qquad (7)$$

where the center-to-center separation $r_{ij} = |r_i - r_j| = [\rho^2 + (z_i - z_j)^2]^{1/2}$, and θ is the angle between the field and the separation vector r_{ij} (see Figure 1). Here, $\rho = [(x_i - x_j)^2 + (y_i - y_j)^2]^{1/2}$ stands for the distance between chain A and chain B (Figure 2), and z_i denotes the vertical shift of the position of microparticles. Since the inverse ferrofluid is confined between two plates, the microparticle dipole at (x, y, z) and its images at $(x, y, 2Lj \pm z)$ for $j = \pm1, \pm2, \ldots$ constitute an infinite chain. In this work, we would discuss the physical infinite chains. After applying a strong magnetic field, the mismatch between the spheres and the host ferrofluid, as well as the different sizes of the two sorts of spheres will make the spheres aggregate into lattices like a bct (body-centered tetragonal) lattice. In fact, the bct lattice can be regarded as a compound of chains of A and B, where chains B are obtained from chains A by shifting a distance r_1 (microparticle radius) in the field direction. Thus, we shall study the case in which the identical nonmagnetic microparticles gather together to form a uniform chain, when phase separation or transition happens. For long range interactions, the individual colloidal microparticles can be made nontouching when they are charged and stabilized by electric or magnetic static forces, with a low volume fraction of nonmagnetic microparticles. The interaction energy between the nonmagnetic microparticles can be divided into two parts: one is from the self-energy of one chain (U_s); the other is from the interaction between different chains ($U_{ij}(\rho, z)$). Consider the nonmagnetic microparticles along one chain at $r_j = 2aj\hat{z}$ ($j = 0, \pm1, \pm2, \ldots$) (namely, chain A), and the other chain at $r_j = (2j + 1)a\hat{z}$ (chain B); the average self-energy per microparticle in an infinite chain is $U_s = -\mu \sum_{s=1}^{\infty}[1/(2as)^3 + 2\sum_l f(l)/(2as)^{2l+4}]$.

If we notice that for an infinite chain all even mulitipole contributions vanish because of spatial magnetic antisymmetry around the spheres, the sum starts at $l = 3$. Because the radius of the sphere is smaller than the lattice parameter a, for large multipole moment, $(r_1^{2l+1} + r_2^{2l+1})/(2a)^{2l} \ll 1$, we need only consider the first two moment contributions for simplicity. Thus, the average self-energy U_s can be calculated as $U_s = -2\mu[\zeta(3)/(2a)^3 + f(3)\zeta(6)/(2a)^6 + f(5)\zeta(10)/(2a)^{10}] = -\mu[0.300514/a^3 + 0.0317920f(3)/a^6 + 0.00195507f(5)/a^{10}]$, where $\zeta(n) = \sum_{s=1}^{\infty} 1/s^n$ is the Riemann ζ function. The interaction energy between two parallel infinite chains can be given by $1/2U_{ij}(\rho, z)$, in which the microparticles along one chain locate at $r_j = 2aj\hat{z}$ ($j = 0, \pm1, \pm2, \ldots$) and one microparticle locates at $r_j = \rho + z\hat{z}$,

$$U_{ij}(\rho, z) = -\mu\left[\left(2 + \rho\frac{\partial}{\partial\rho}\right)\sum_{j=-\infty}^{\infty}\frac{1}{[\rho^2 + (z - 2ja)^2]^{3/2}}\right] - \mu\left[\sum_l f(l)\left(2 + \frac{3}{2l+2}\rho\frac{\partial}{\partial\rho}\right)\sum_{j=-\infty}^{\infty}\frac{1}{[\rho^2 + (z - 2ja)^2]^{l+2}}\right] = U_1 + U_2 \qquad (8)$$

Following the Fourier expanding technique which is proposed by Tao et al.,[27] we derive U_2 which is the second part of $U_{ij}(\rho, z)$ as

$$U_2 = -\mu\sum_l \frac{f(l)}{4a\rho^{2l+3}}\left[-\frac{(2l+1)\sqrt{\pi}\Gamma\left(l + \frac{3}{2}\right)}{\Gamma(l+3)} + 2^{1/2-l}\left(\frac{s\rho}{a}\right)^{l+3/2}\pi^{l+2}\cos\left(\frac{s\pi z}{a}\right)\cdot S\right] \qquad (9)$$

with

$$S = \sum_{s=1}^{\infty}\left(\frac{K_{5/2}\left(\frac{s\pi}{\rho}\right)}{\Gamma(l+3)} + \frac{4K_{3/2}\left(\frac{s\pi}{\rho}\right)}{\Gamma(l+2)}\right) \qquad (10)$$

Here, $K_i(x)$ represents the ith order modified Bessel function, $\Gamma(x)$ is the Γ function, and s denotes the index in Fourier transformation.[26] And the dipole−dipole energy U_1 is written as

$$U_1 = -\frac{\mu}{a^3}\sum_{s=1}^{\infty} 2\pi^2 s^2 K_0\left(\frac{s\pi\rho}{a}\right)\cos\left(\frac{s\pi z}{a}\right) \qquad (11)$$

We obtain the expression for $U_{ij}(\rho, z)$, and the interaction energy per nonmagnetic microparticle $U(\rho, z)$ is $U_s + (1/2)\sum_k U_{ij}(\rho, z)$, where $\sum_k$ denotes the summation over all chains except the considered microparticle. For the same reason of approximation discussed above, we need only choose the first two terms ($l = 3$ and $l = 5$) in the calculation.

The interaction between chain A and chain B depends on the shift z, the lattice structure, and the nonmagnetic microparticle size. An estimation of the interaction energy per nonmagnetic microparticle includes the nearest and next-nearest neigh-

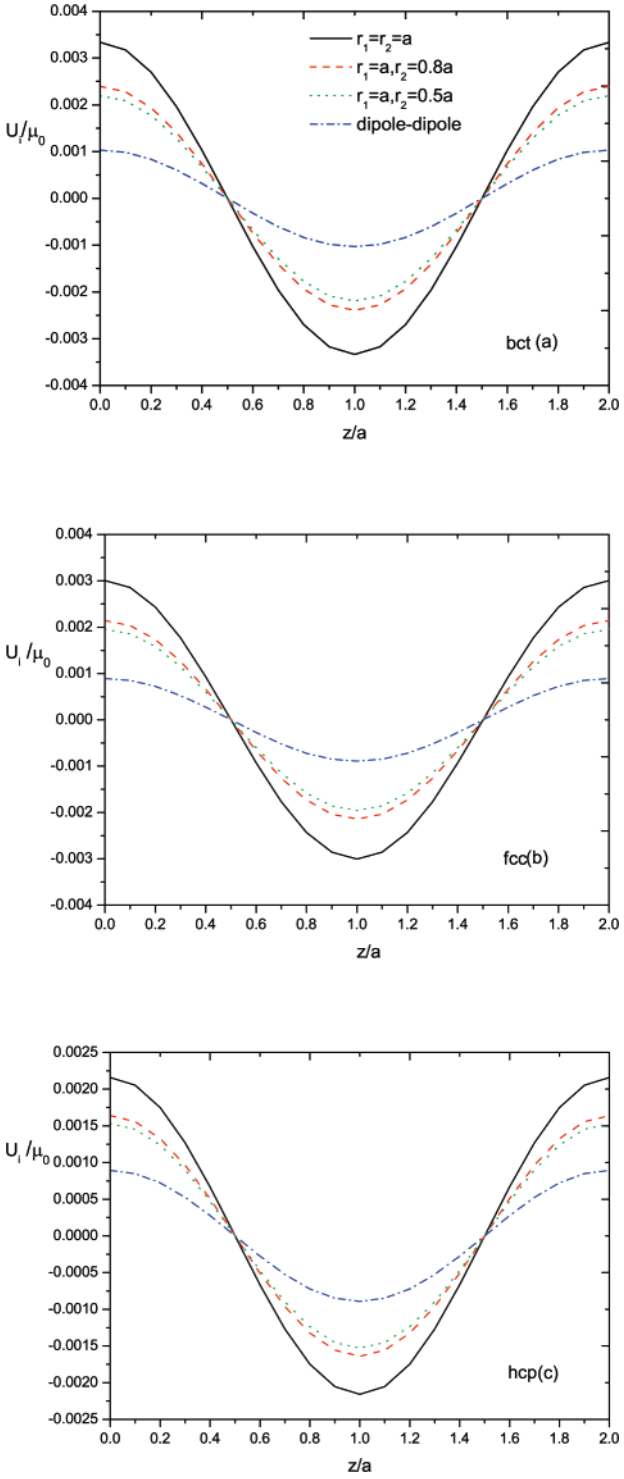

Figure 3. Dependence of interaction energy $U_l(\rho, z)$ (in units of μ_0) versus vertical shift z for different lattices: (a) bct, (b) fcc, and (c) hcp. In the legend, "dipole−dipole" denotes the case that the dipole−dipole interaction is only considered for calculating the interaction energy.

boring chains; here, we could discuss three most common lattice structures: bct, fcc, and hcp lattices. For the above lattices, their corresponding energy of $U_{ij}(\rho, z)$ can be respectively approximated as $U_{ij,\mathrm{bct}}(\rho, z) = 4U_{ij}(\sqrt{3}a, z = 0) - 4U_{ij}(\sqrt{6}a, z = 0)$, $U_{ij,\mathrm{fcc}}(\rho, z) = 4U_{ij}(\sqrt{3}a, z = 0) - 2U_{ij}(2a, z = 0)$, and $U_{ij,\mathrm{hcp}}(\rho, z) = 3U_{ij}(\sqrt{3}a, z = 0) - 4U_{ij}(2a, z = 0)$.

Figure 3 shows, for different lattices, the dependence of $U_{ij}(\rho, z)$ on the vertical position shift z, which determines whether the interaction is attractive or repulsive. $U_{ij}(\rho, z)$ reflects the

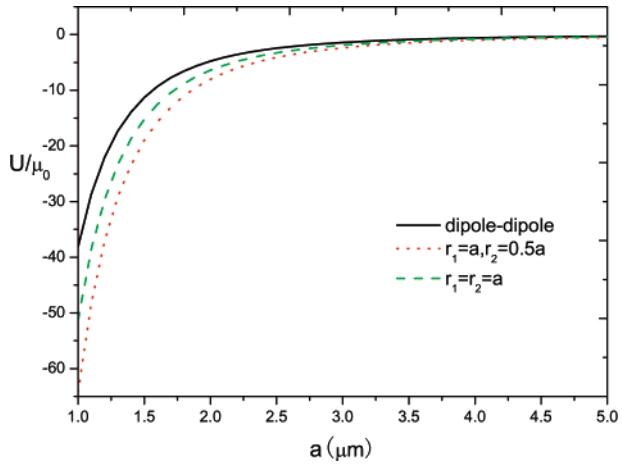

Figure 4. Interaction energy $U(\rho, z)$ versus lattice constant a. The solid line stands for the case in which the dipole−dipole interaction is only considered.

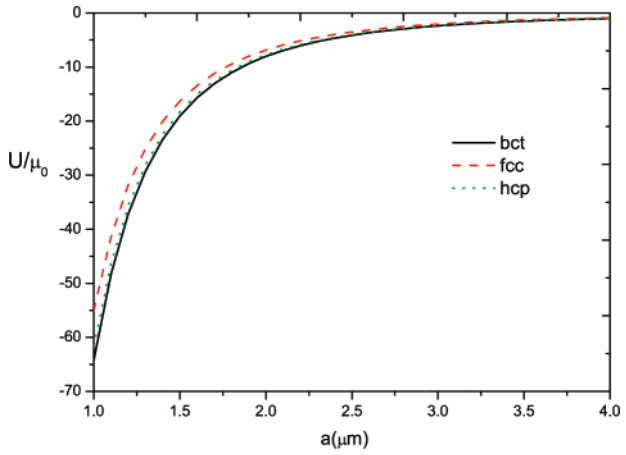

Figure 5. Interaction energy per microparticle $U(\rho, z)$ versus lattice constant a for different lattices, bct, fcc, and hcp.

energy difference between chain A and chain B for (a) bct, (b) fcc, and (c) hcp lattices. It is evident that, for the same lattice structure, $U_{ij}(\rho, z)$ is minimized when the size difference between chain A and chain B is the smallest. For the sake of comparison, we also plot the results obtained by considering the dipole−dipole interaction only. Comparing the different lattices, we find that the bct lattice possesses the smallest energy at the equilibrium point, thus being the most stable.

Figure 4 displays the interaction energy $U(\rho, z)$ as a function of the lattice constant a for the bct lattice. It is shown that as the lattice constant increases, the dipole-multipole effect becomes weaker and weaker, and eventually it reduces to the dipole−dipole effect. In other words, as the lattice constant is smaller, one should take into account the dipole-multipole effect. In this case, the effect of polydispersity in size can also play an important role.

Figure 5 displays the interaction energy per nonmagnetic microparticle $U(\rho, z)$ versus the lattice parameter a for different lattice structures. The bct structure also proves to be the most stable state while the hcp lattice has the highest energy. It also shows that the energy gap between bct lattice and fcc lattice exists but is small. Figure 6a shows that the energy gap $\Delta U = U_{\mathrm{bct}} - U_{\mathrm{fcc}}$ is about 0.5% of the interaction energy value. In this aspect, the bct lattice proves always to be a more stable structure comparing with fcc. As the radius of microparticles increases, the energy gap between bct and fcc lattice enlarges accordingly. That is, the bct lattice becomes much more stable.

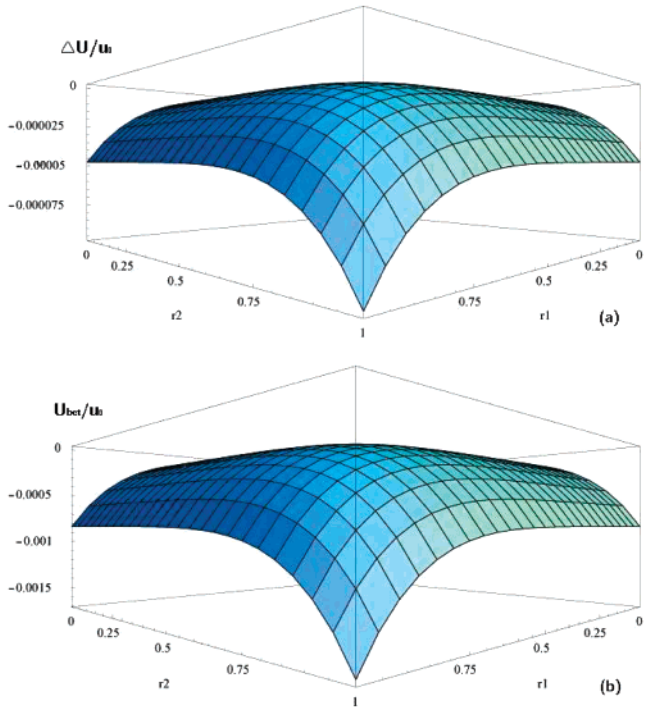

Figure 6. (a) Energy gap $\Delta U = U_{bct} - U_{fcc}$ (in units of μ_0) versus different size of nonmagnetic microparticles in chain A and chain B; (b) The bct lattice energy $U(\rho, z)$ (in units of μ_0) versus different sizes of nonmagnetic microparticles in chain A and chain B.

Figure 6b shows the bct lattice energy $U(\rho, z)$ in respect of different sizes of microparticles for chain A and chain B. It can be seen that the close touching packing ($r_1 = r_2 = a$) has the lowest energy state. However, also from the graph, the crystal with the same microparticle size (monodisperse system) may not be the lowest energy state, which gives a possible way of fabricating different crystals by tuning the distribution of microparticle size.

IV. Polydisperse System with Random Distributions

In section III, we have discussed the structure and interaction in a bidisperse inverse ferrofluid (namely, containing microparticles with two different sizes). But the interaction form in a polydisperse crystal system is complex and sensitive to the microstructure in the process of crystal formation. Now, we investigate the structure of polydisperse inverse ferrofluids with microparticles of different sizes in a random configuration. To proceed, we assume that the average radius r satisfies the Gaussian distribution

$$P(r) = \frac{1}{\sqrt{2\pi}\sigma} \exp\left(-\frac{(r - r_0)^2}{2\sigma^2}\right) \qquad (12)$$

where σ denotes the standard deviation of the distribution of microparticle radius, which describes the degree of polydispersity. Integrating eq 9 by r_1 and r_2, we could get the average dipole−multipole energy $\bar{U}_2$. Doing the same calculation to self-energy U_s, we can get the average interaction energy $\bar{U}(\rho, z) = \bar{U}_s + U_1 + \bar{U}_2$, where the microparticle size r_1 and r_2 are replaced by the mean radius r_0. The microparticle sizes will be distributed in a wider range as long as a larger σ is chosen.

Figure 7a shows the ground state interaction energy of bct lattice for different polydisperse distributions. As the degree of polydispersity σ increases, the energy $U(\rho, z)$ drops fast, especially when the distribution of microparticle size gathers

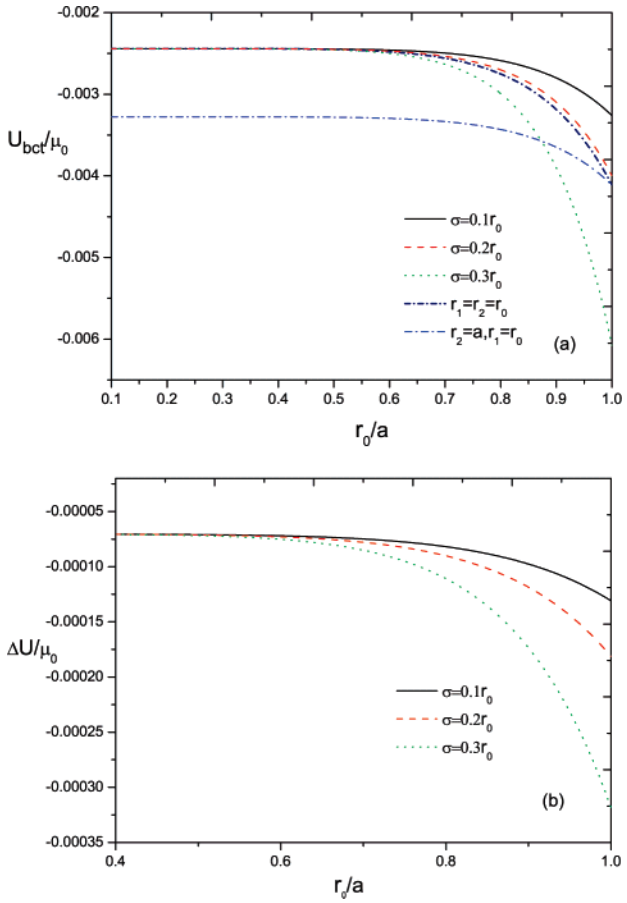

Figure 7. (a) Ground state interaction energy of a bct lattice versus microparticle size r_0 for random polydispersity configuration (solid, dashed, and dotted lines) and a configuration composed of two different uniform chains (dash-dotted and short-dash-dotted lines). (b) The energy gap ΔU between bct and fcc lattices for random polydispersity versus r_0.

around $r = a$. It shows that the inverse ferrofluid crystal in the formation of ground state tends to include microparticles possessing more different sizes. The crystal configuration energy of two uniform chains with identical microparticle aggregation is also plotted in the graph. Here, we consider two cases. First, we assume the microparticles in chain A and chain B are identical, $r_1 = r_2 = r_0$. As r_0 increases, the behavior of energy decreasing is discovered to be similar with the random configuration with $\sigma = 0.2r_0$. Second, we set for one chain, such as chain B, the microparticle size $r_2 = a$ to be unchanged, while the microparticle size r_1 of chain A increases. It shows that the bct lattice energy for the second case is lower than the first case and two other random configurations. And it also shows that the random configuration is not always the state with the lowest energy. It proves that polydisperse systems are sensitive to many factors which can determine the microstructure. Figure 7b shows the energy gap between bct and fcc lattices for different distribution deviation σ. It is evident that higher σ leads to larger energy difference between bct and fcc, especially at larger r_0. In other words, at larger r_0 and/or σ, bct lattices are much more stable than fcc.

V. Molecular Dynamics Simulations

Here, we use a molecular dynamics simulation, which was proposed by Tao et al.,[28] in order to briefly discuss the structure formation of bidisperse inverse ferrofluids. The simulation herein involves dipolar forces, multipole forces, viscous drag forces,

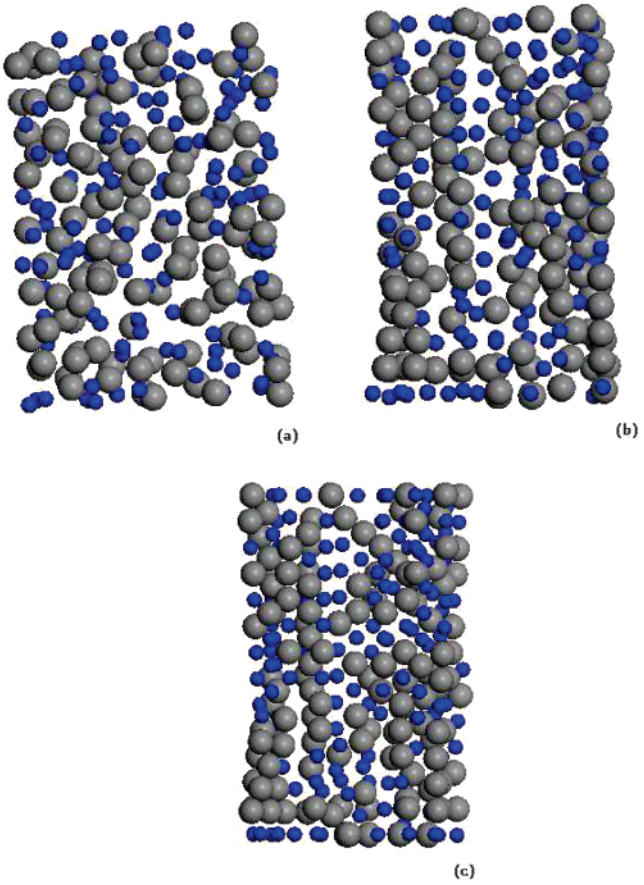

Figure 8. Configuration of nonmagnetic microparticle distribution at (a) the initial state, (b) the state after 15 000 time steps, and (c) the state after 80 000 time steps.

and the Brownian force. The microparticles are confined in a cell between two parallel magnetic pole plates, and they are randomly distributed initially, as shown in Figure 8a. The motion of a microparticle i is described by a Langevin equation,

$$m_a \frac{d^2\vec{r}_i}{dt^2} = \vec{F}_i - 3\pi\sigma\eta \frac{d\vec{r}_i}{dt} + \vec{R}_i(t) \tag{13}$$

where the second term in the right-hand side is the Stokes's drag force, R_i is the Brownian force, and

$$F_i = \sum_{i \neq j} (f_{ij} + f_{ij}^{rep}) + f_i^{wall} \tag{14}$$

Here, $f_{ij} = -\nabla U(\rho, z)$, while f_{ij}^{rep}, f_i^{wall}, and $R_i(t)$, have the similar expressions as those in ref 27 and the references therein. In eq 13, m_a and σ are respectively the average mass and diameter of microparticles. Figure 8 shows the inverse ferrofluid structure with the parameters, magnetic field $H = 14$ Oe, temperature $T = 300$ K, $A' \equiv \mu_f m_1 m_2/3\pi^2\sigma^6\eta^2 m_a = 10^{-2}$, and $B' \equiv (\sqrt{6\pi k_B T\sigma^9\eta/\tau})/3\mu_f m_1 m_2 = 10^{-4}$. Here, A' denotes the ratio of a dipolar force to a viscous force, B' is the ratio of Brownian force to a dipolar force, k_B is the Boltzmann constant, and τ is the subinterval time step.

We take into account a bidisperses system that contains two kinds of microparticles with different sizes, as shown in Figure 8. In details, this figure displays the configuration of microparticle distribution in a bidisperse system at (a) the initial state, (b) the state after 15 000 time steps, and (c) the state after 80 000 time steps. The order of Figure 8c is better than that of Figure 8b. Here, we should remark that 80 000 steps give the sufficient long time steps to reach the equilibrium state for the case of our interest. The structure for the bidisperse system in Figure 8b,c has the following features: (i) In the field direction, the large spheres form the main chains from one plate to the other, where the large spheres touch each other. (ii) The large spheres also form many small bct lattice grains. However, they do not form a large bct lattice. (iii) The small spheres fill the gaps between these bct lattice grains. From Figure 8, it is observed that, for the parameters currently used, the order of a bidisperse system (which is a bct-like structure) is not as good as that of monodisperse system (no configurations shown herein). We should remark that the long-range interaction can yield the above-mentioned bct lattice structure, but some perturbations caused by the Brownian movement existing in the system can change it to another lattice structure which has similar free energy. Therefore, for the bidisperse system of our interest, the large spheres form the main chains from one plate to the other in the field direction, thus forming many small bct-like lattice structures. While small spheres fill the gaps between these bct-like lattices, they themselves do not form a bct-like lattice because of such perturbations. Here, we should also mention that the degree of order of a specific system depends on the choice of various physical parameters, for example, the size of microparticles and so forth.

VI. Summary

In summary, by using theoretical analysis and molecular dynamics simulations, we investigate the structure of colloidal crystals formed by nonmagnetic microparticles (or magnetic holes) suspended in a host ferrofluid, by taking into account the effect of polydispersity in size of the nonmagnetic microparticles. We obtain an analytical expression for the interaction energy of monodisperse, bidisperse, and polydisperse inverse ferrofluids. The bct lattices are shown to possess the lowest energy when compared with other sorts of lattices and thus serve as the ground state of the systems. Also, the effect of microparticle size distributions (namely, polydispersity in size) plays an important role in the formation of various kinds of structural configurations. Thus, it seems possible to fabricate colloidal crystals by choosing appropriate polydispersity in size. As a matter of fact, it is straightforward to extend the present model to more ordered periodic systems,[29] in which the commensurate spacings can be chosen as equal or different.

Acknowledgment. Two of us (Y.C.J. and J.P.H.) are grateful to Dr. Hua Sun for valuable discussion. This work was supported by the National Natural Science Foundation of China under Grant 10604014, by the Shanghai Education Committee, and the Shanghai Education Development Foundation ("Shu Guang" project), by the Pujiang Talent Project (No. 06PJ14006) of the Shanghai Science and Technology Committee, and by Chinese National Key Basic Research Special Fund under Grant 2006CB921706. Y.C.J. acknowledges the financial support by Tang Research Funds of Fudan University and by the "Chun Tsung" Scholar Program of Fudan University.

References and Notes

(1) Odenbach, S. *Magnetoviscous Effects in Ferrofluids;* Springer: Berlin, 2002.

(2) Meriguet, G.; Cousin, F.; Dubois, E.; Boue, F.; Cebers, A.; Farago, B.; Perzynski, W. *J. Phys. Chem. B* **2006**, *110*, 4378.

(3) Sahoo, Y.; Goodarzi, A.; Swihart, M. T.; Ohulchanskyy, T. Y.; Kaur, N.; Furlani, E. P.; Prasad, P. N. *J. Phys. Chem. B* **2005**, *109*, 3879.

(4) Toussaint, R.; Akselvoll, J.; Helgesen, G.; Skjeltorp, A. T.; Flekkøy, E. G. *Phys. Rev. E* **2004**, *69*, 011407.
(5) Skjeltorp, A. T. *Phys. Rev. Lett.* **1983**, *51*, 2306.
(6) Zubarev, A. Y.; Iskakova, L. Y. *Physica A* **2003**, *335*, 314.
(7) Chantrell, R.; Wohlfart, E. *J. Magn. Magn. Mater.* **1983**, *40*, 1.
(8) Rosensweig, R. E. *Annu. Rev. Fluid Mech.* **1987**, *19*, 437.
(9) Ugelstad, J.; Stenstad, P.; Kilaas, L.; Prestvik, W. S.; Herje, R.; Berge, A.; Hornes, E. *Blood Purif.* **1993**, *11*, 349.
(10) Hayter, J. B.; Pynn, R.; Charles, S.; Skjeltorp, A. T.; Trewhella, J.; Stubbs, G.; Timmins, P. *Phys. Rev. Lett.* **1989**, *62*, 1667.
(11) Koenig, A.; Hébraud, P.; Gosse, C.; Dreyfus, R.; Baudry, J.; Bertrand, E.; Bibette, J. *Phys. Rev. Lett.* **2005**, *95*, 128301.
(12) Zhang, H.; Widom, M. *Phys. Rev. E* **1995**, *51*, 2099.
(13) Friedberg, R.; Yu, Y. K. *Phys. Rev. B* **1992**, *46*, 6582.
(14) Clercx, H. J. H.; Bossis, G. *Phys. Rev. B* **1993**, *48*, 2721.
(15) Mondain-Monval, O.; Leal-Calderon, F.; Philip, J.; Bibette, J. *Phys. Rev. Lett.* **1995**, *75*, 3364.
(16) Sacanna, S.; Philipse, A. P. *Langmuir* **2006**, *22*, 10209.
(17) Claesson, E. M.; Philipse, A. P. *Langmuir* **2005**, *21*, 9412.
(18) Dai, Q. Q.; Li, D. M.; Chen, H. Y.; Kan, S. H.; Li, H. D.; Gao, S. Y.; Hou, Y. Y.; Liu, B. B.; Zou, G. T. *J. Phys. Chem. B* **2006**, *110*, 16508.
(19) Ethayaraja, M.; Dutta, K.; Bandyopadhyaya, R. *J. Phys. Chem. B* **2006**, *110*, 16471.
(20) Jodin, L.; Dupuis, A. C.; Rouviere, E.; Reiss, P. *J. Phys. Chem. B* **2006**, *110*, 7328.
(21) Gao, L.; Li, Z. Y. *J. Appl. Phys.* **2002**, *91*, 2045.
(22) Wei, E. B.; Poon, Y. M.; Shin, F. G.; Gu, G. Q. *Phys. Rev. B* **2006**, *74*, 014107.
(23) Kristóf, T.; Szalai, I. *Phys. Rev. E* **2003**, *68*, 041109.
(24) Huang, J. P.; Holm, C. *Phys. Rev. E* **2004**, *70*, 061404.
(25) Černák, J.; Helgesen, G.; Skjeltorp, A. T. *Phys. Rev. E* **2004**, *70*, 031504.
(26) Jackson, J. D. *Classical Electrodynamics*, 3rd ed.; Wiley: New York, 1999; Chapter 4.
(27) Tao, R.; Sun, J. M. *Phys. Rev. Lett.* **1991**, *67*, 398.
(28) Tao, R.; Jiang, Q. *Phys. Rev. Lett.* **1994**, *73*, 205.
(29) Gross, M.; Wei, C. *Phys. Rev. E* **2000**, *61*, 2099.